A Parallel Manipulator for Mobile Manipulating UAVs

Todd W. Danko[1], Kenneth P. Chaney[2] and Paul Y. Oh[3]

Abstract— **Manipulating objects using arms mounted to unmanned aerial vehicles (UAVs) is attractive because UAVs may access many locations that are otherwise inaccessible to traditional mobile manipulation platforms such as ground vehicles. Most previous efforts seeking to coordinate the combined manipulator-UAV system have focused on using a manipulator to extend the UAV's reach and assume that the both the UAV and manipulator reliably reach commanded goal poses.**

This work accepts the reality that state of the art UAV positioning precision is not of a high enough quality to reliably perform simple tasks such as grasping objects. A six degree of freedom parallel manipulator is servoed to precise goal locations, compensating for UAV positioning errors while the UAV is driven to keep the manipulator within reach of its goal.

A description of a parallel manipulator that is suitable for such an application and experimental performance results are presented.

I. Introduction

Unmanned Aerial Vehicles (UAVs) were originally deployed as target drones for combat pilot training but have evolved over time to provide valuable roles in intelligence, surveillance and reconnaissance for both civilian and military operations. Historically, UAVs were built and operated in ways to avoid interacting with their environment's at all costs, affording them the ability to quickly and efficiently travel large distances. The ability for aerial vehicles to manipulate or carry objects that they encounter could greatly expand the types of missions achievable by unmanned aerial systems. High degree of freedom (DOF) robots with dexterous arms could lead to transformative applications such as material handling for infrastructure repair, law enforcement, disaster response, casualty extraction, and personal assistance leading to a paradigm shift in the way UAVs are deployed. Such aerial manipulation systems are referred to as Mobile Manipulating Unmanned Aerial Vehicles (MM-UAV).

Several aircraft-manipulator configurations exist to create aerial manipulation systems:

Single DOF Aerial Grasping: Substantial work including [1]–[5] has been conducted on the use of single degree of freedom grippers mounted rigidly to aerial platforms. These platforms rely on the assumption that the positioning accuracy of the UAV is adequate to perform any necessary manipulations. The use of motion capture systems to ensure highly precise positioning has been employed by many, while a few groups including [6] have employed large, compliant grippers to forgive positioning errors while performing simple grasps.

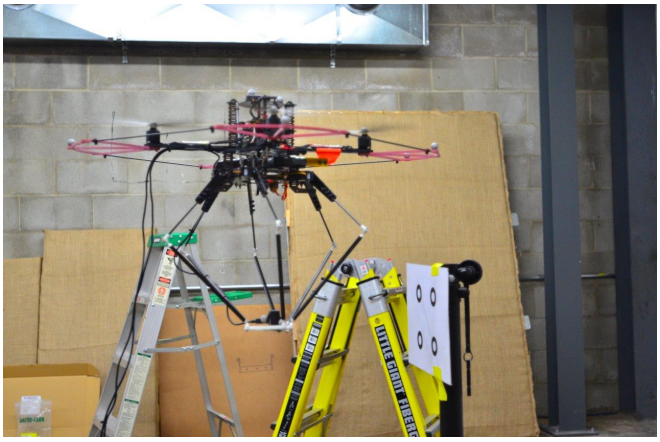

Fig. 1. Envisioned aerial manipulation system featuring a 6-DOF parallel manipulator to compensate for host UAV imprecision

Non-Redundant Articulated Aerial Manipulation: Another approach to creating an aerial manipulation system is to augment a six DOF UAV with an arm that has, or makes use of, fewer than six DOFs as explored by [7]–[14]. This approach assumes that the each non-redundant degree of freedom from the UAV and manipulator can be controlled precisely enough to perform the desired manipulation, but what happens when the UAV's position is perturbed by wind gusts, or imperfect state estimation? If these perturbations cannot be compensated for by the manipulator's DOFs, they are transmitted through the system, diminishing end-effector precision.

Fully-Redundant Articulated Aerial Manipulation: Attaching a six DOF arm to a quadrotor UAV allows the UAV to be used in a way that crudely positions the manipulator so that the desired end-effector position is within reach of a target. The manipulator can then use its six DOFs to both finely position the end-effector and compensate for unintended motions of the UAV. This approach does however, require a manipulator with six DOFs, which introduces integration challenges as traditional designs for such manipulators are bulky–causing problems during take off and landing and heavy with large moving masses–disrupting UAV stability.

UAV Precision: Aerial manipulation approaches that make use of manipulators that cannot move to offset undesirable UAV motions are forced to accept the degree of precision

This work was supported in part by the National Science Foundation (NSF) award CNS-1205490. Any opinion, findings, and conclusions or recommendations expressed in this material are those of the authors and do not necessarily reflect the views of NSF.

[1]Todd W. Danko is a Lead Research Scientist at Lockheed Martin's Advanced Technology Laboratories, todd.w.danko@lmco.com

[2]Kenneth P. Chaney is a student at Drexel University in the Department of Computer Engineering, kpc49@drexel.edu

[3]Paul Y. Oh the Director of the Drones and Autonomous Systems Lab at the University of Nevada, Las Vegas, paul.oh@unlv.edu

TABLE I

PUBLISHED BENCHMARK STATION KEEPING PERFORMANCE WHILE HOVERING [15] UTILIZING VSLAM

Venue	RMS error (m)	Test altitude (m)
indoor x/y	0.069	1.4
indoor z	0.009	1.4
outdoor x/y	0.44	3.3
outdoor z	0.11	3.3

possible for the host UAV, at least for some directions. While many groups rely on highly precise motion capture systems to achieve extremely accurate knowledge of the aerial manipulator's position, perturbations from air currents and even motions of the aerial manipulators's own arm make achieving precise goal positions difficult.

Table I shows a published benchmark for UAV precision utilizing VSLAM both indoors and outdoors [15], which is considered state of the art for field deployed UAVs.

The RMSE (1σ, assuming a Gaussian distributions) values, in Table I, show how far from the goal position the center of the quadrotor will be 65% of the time; thus if a manipulator is designed that has a workspace that is able to reach a 2σ deviation it will be able to compensate for UAV positioning imperfections 95% of the time. Continuous position compensation is necessary to achieve this performance, so the manipulator must have a continuous workspace. The update speed of the manipulator for small motions within the workspace must be fast enough that the movement of the UAV doesn't have an impact on the location of the end-effector.

Partitioning the task of manipulation leads to several design constraints imposed upon the manipulator:

1) It must be able to compensate for the dimensions of the UAV imprecision
2) It must be dynamically faster than the UAV
3) It must not interfere with the UAV while taking off, landing, or flying

II. PARALLEL MANIPULATOR

The current aerial manipulation paradigm is to use the degrees of freedom (DOF) of the vehicle to at least partially position the end-effector. This paradigm produces a system that isn't capable of precise positioning of the end-effector, and in turn leads to the need for large grippers to overcome positioning imperfections while performing simple tasks such as grasping. The goal of this parallel manipulator is to overcome the imperfections of a quadrotor's positioning capabilities with a system that allows for high frequency changes in the pose of the end-effector. This will allow for more precise placement of the end-effector. The envisioned system is shown in Figure 1 and uses a parallel manipulator to allow for 6 DOF motions from the base of the quadrotor, precisely positioning the end-effector relative to a target of interest.

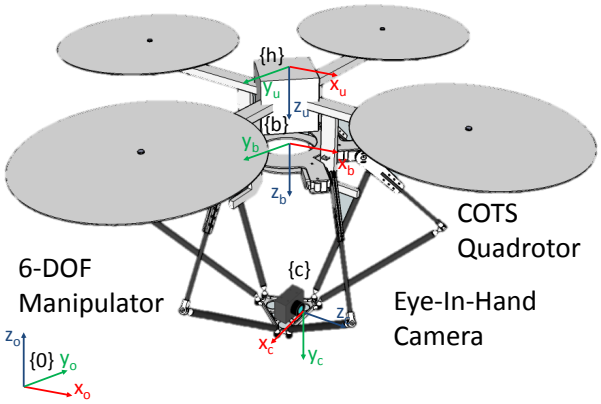

Fig. 2. Model of quadrotor coupled to a six DOF parallel manipulator with eye-in-hand camera

The aerial manipulation system performs a form of partitioned control [16], taking advantage of a Multi-In-Multi-Out (MIMO) control loop. The parallel manipulator is driven to minimize an error between its end-effector pose with regard to a world goal regardless of UAV motions. The UAV's velocity is simultaneously servoed using the pose of the manipulator as a kinematic sensor. The UAV is driven to move the base of the manipulator such that the end-effector has an affinity for the center of its reachable workspace. This ensures that the manipulator is capable of rejecting unexpected host UAV position perturbations. A low level autopilot us used to stabilize the aerial manipulation system, taking advantage of low frequency reference position such as VSLAM, GPS or degraded MoCap in conjunction with high frequency inertial, angular rate, barometric and magnetometer sensors.

Several shortcomings of a serial link manipulator have been identified when cast in the context of integrating it with a quadrotor UAV. Specifically, the design of the serial link manipulator, as described in [**?**], required the servo motors located at the root of the arm to be strong enough to effectively drive the mass and inertia of each subsequent link toward the end-effector of the arm, resulting in the necessary selection of large, heavy motors. These limitations motivated the evaluation of alternate manipulator designs for MM-UAV, including parallel mechanisms such as Stewart platforms [17]. A parallel manipulator was designed with six legs attaching the base to a moving platform. Each leg has one driven revolute joint and two universal joints (6-RUU) as shown in Figure 2. The application of a full six DOF parallel manipulator is novel to this work, though a three DOF delta robot mechanism was described in [18] for use in aerial contact inspection missions.

III. PARALLEL MANIPULATOR MODEL

The parallel manipulator as shown in Figure 3 is composed of a base, b, a moving top platform, p and six legs. Each leg,

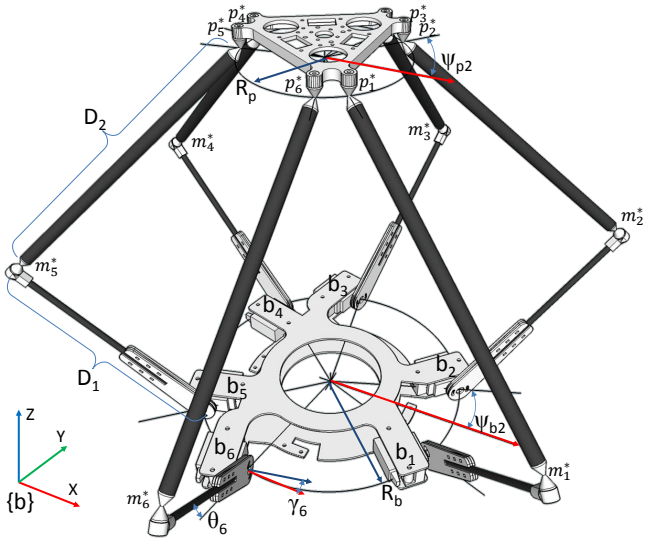

Fig. 3. Dimensions and angles defining the parallel manipulator (inverted for clarity)

TABLE II

PHYSICAL PROPERTIES OF THE PARALLEL MANIPULATOR

Symbol	Value	Description
D_1	0.1683 m	Fixed length link connecting base joint to knee
D_2	0.2156 m	Fixed length link connecting knee to top platform joint
R_b	0.1035 m	Radius from the center of the base platform to each leg attachment point
R_p	0.0500 m	Radius from the center of the top platform to each leg attachment point
M_b	270 g	Mass of base assembly, one unit rigidly fixed to host platform
M_p	40 g	Mass of moving platform with camera one unit, moves relative to base
M_1	12 g	Mass of each moving link connecting base joint to knee, six units
M_2	11 g	Mass of each moving link connecting knee joint to top platform, six units
M_t	454 g	Total mass of manipulator assembly
M_m	184 g	Total mass of moving components

i, is attached to the base by a revolute joint which rotates to a commanded value of θ_i around an axis defined by an angle γ_i that departs from the leg's point of attachment to the base at points listed in Table IV. The revolute joint for each leg drives a fixed length link, D_1, leading to a universal joint knee, which is connected to the top platform by another fixed length link, D_2, and another universal joint.

Knowing the radius of the base attachment points, R_b, the coordinates of each leg's attachment to the base, in manipulator base coordinates, can be calculated using Equation 1 to generate the left side of Table IV.

$$b_i = [b_{xi}, b_{yi}, b_{zi}]^T = [R_b \cos(\psi_{bi}), R_b \sin(\psi_{bi}), 0]^T \quad (1)$$

Likewise, knowing the radius of the top platform attachment points, R_p, the coordinates of each leg's attachment to the top platform, in top platform coordinates, can be

TABLE III

ANGULAR COORDINATES OF LEG ATTACHMENT POINTS TO THE BASE AND MOVING PLATFORM

leg (i)	ψ_{bi} $(radians)$	γ_i $(radians)$	ψ_{pi} $(radians)$
1	6.0214	6.5450	0.8727
2	0.2618	0.7854	1.2217
3	1.8326	2.3562	2.9671
4	2.3562	2.8798	3.3161
5	3.9270	4.4506	5.0615
6	4.4506	4.9742	5.4105

TABLE IV

LEG ATTACHMENT POSITIONS TO THE TOP AND BASE IN MANIPULATOR BASE COORDINATES

	Base Connections			Top Connections		
i	b_{xi} (m)	b_{yi} (m)	b_{zi} (m)	p_{xi} (m)	p_{yi} (m)	p_{zi} (m)
1	0.1000	−0.0268	0	0.0321	−0.0383	0
2	0.1000	0.0268	0	0.0321	0.0383	0
3	−0.0268	0.1000	0	0.0171	0.0470	0
4	−0.0732	0.0732	0	−0.0492	0.0087	0
5	−0.0732	−0.0732	0	−0.0492	−0.0087	0
6	−0.0268	−0.1000	0	0.0171	−0.0470	0

calculated using Equation 2 to generate right side of Table IV.

$$p_i = [p_{xi}, p_{yi}, p_{zi}]^T = [R_p \cos(\psi_{pi}), R_p \sin(\psi_{pi}), 0]^T \quad (2)$$

IV. PARALLEL MANIPULATOR INVERSE KINEMATICS

The goal of inverse kinematics calculations for this parallel manipulator is to identify goal angles for each of the six driven revolute joints around the platform's base that will drive the top platform to a desired $SE(3)$ pose in the manipulator's base coordinates.

Given a goal pose represented by a homogeneous transform, ${}^bT_p$ relative to the parallel manipulator's base, the first step is to calculate each leg's attachment point to the top platform, p_i, translated to it's goal pose, $p_i^\star$, in manipulator base coordinates as shown in Equation 2.

$$p_i^\star = p_i {}^bT_p \quad (3)$$

Next, the Euclidean distance, $L_i^\star$, is calculated for for each leg as the direct distance between each base attachment point, b_i, and desired top platform attachment point, $p_i^\star$. $L_i^\star$ is a virtual leg of a triangle formed by each leg between the b_i, $p_i^\star$ and the knee, $m_i^\star$.

$$L_i^\star = \sqrt{(p_{xi}^\star - b_{xi})^2 + (p_{yi}^\star - b_{yi})^2 + (p_{zi}^\star - b_{zi})^2} \quad (4)$$

Finally, the angle of each driven joint, θ_i, is calculated using Equation 5.

$$\theta_i = \arcsin\left(\frac{c}{\sqrt{a^2 + b^2}}\right) - \arctan\left(\frac{b}{a}\right) \quad (5)$$

Where:

$a = 2D_1(p_{zi}^\star - b_{zi})$

$b = 2D_1 \sin(\gamma_i)(p^\star_{xi} - b_{xi}) - \cos(\gamma_i)(p^\star_{yi} - b_{yi})$
$c = L_i^{*2} - D_2^2 + D_1^2$

V. Parallel Manipulator Design Criteria

Several factors were considered while designing the parallel manipulator mechanism, driven by the device's intended use. Foremost, it is desirable to fly the manipulator on a Pelican quadrotor, so the manipulator must be light enough to be carried by this platform, therefore the target weight is less than $0.6\ kg$. Further, there is a desire to minimize the moving mass of the system, which is one of the motivations for using a parallel design that allows all of the motors to be mounted rigidly to the host UAV's body, minimizing the impact of manipulator motions on the host UAV. The resulting system is composed of the items listed in Table II with a total mass of $0.454\ kg$ and a moving mass of $0.184\ kg$.

The shape of the pelican quadrotor provides additional guidance for the layout of the parallel mechanism. The position of each leg's root at the base, ψ_{bi}, and the orientation of the axis that each motor rotates around, γ_i, were selected to ensure that the manipulator's legs do not interfere with the quadrotor's landing legs while in the stowed or deployed configurations.

Further, there is a desire to be able to fold the mechanism flat against the bottom of the Pelican quadrotor to facilitate take off and landing from the ground without special spacers, platforms or retractable landing gear mechanisms. To allow for this, the relationship between D_1 and D_2 was calculated such that:

$$D_2 = ||m_i^\star - b_i|| \tag{6}$$

Where:

$$m_i^\star = \begin{bmatrix} m^\star_{xi} \\ m^\star_{yi} \\ m^\star_{zi} \end{bmatrix} = \begin{bmatrix} D_1 \cos(\theta_i) \sin(\gamma_i) + b_{xi} \\ -D_1 \cos(\theta_i) \cos(\gamma_i) + b_{yi} \\ D_1 \sin(\theta_i) + b_{zi} \end{bmatrix} \tag{7}$$

When each θ_i angle is set to 0.

As a result, the manipulator can stow and deploy for use as captured in the image sequence shown in Figure 4.

Finally, each leg as shown in Figure 2 is constructed to be driven by an off-the-shelf miniature hobby servo [19] capable of providing $0.34\ N-m$ of torque and a maximum rotational velocity of $7.5\ rad/s$. The universal joints located at the knee, $m_i^\star$ and ankle, $p_i^\star$ are created by pulling pointed bearing surfaces together using a spring-tensioned cable that is threaded through the leg assembly. The spring's stretched length varies slightly as these joints are passively driven. Additionally, the spring mechanism allows the parallel manipulator assembly to temporarily deform without being damaged in the event of unexpected stress, such as a crash of the aerial manipulator.

VI. Comparison to Serial Manipulator

This system was compared to a standard 6-DOF serial manipulator outlined in [**?**], that was constructed with standard Dynamixel servos driving the arm, as serial manipulators are currently the state of the art for aerial manipulator. The reachability of the serial manipulator is shown in Figure 5(b); the reachable workspace is mostly in a forward facing direction and doesn't allow for all directions to be equally reachable. Which is a distinct disadvantage because variations in motion can happen in any direction with a quadrotor. In addition to the torque a serial manipulator generates (shown in Figure 6(b)) on the quad rotor makes it difficult to actually fly and effectively compensate for the variations of the quad rotor which could happen in any direction. The reachability maps in Figure 5(a) show that the parallel manipulator has a very uniform reachable volume around the center of the vehicle.

TABLE V
Experimentally derived dynamic characterizations of the host UAV and parallel and serial manipulators

Parameter	Bandwidth (Hz)	Rise Time (s)	Settle Time (s)
UAV X-Y	0.28	1.65	8.29
UAV Z	0.36	1.03	1.45
Parallel Manipulator X-Y	0.66	0.64	3.36
Parallel Manipulator Z	0.69	0.68	3.67
Serial Manipulator X-Y	0.42	0.78	4.94
Serial Manipulator Z	0.45	0.65	5.92

A. Dynamic Characterization

VII. Flight Test Results

Several experiments were conducted to evaluate the performance of the parallel manipulator equipped quadrotor in maintaining an end-effector pose relative to fixed targets. For these experiments, the custom manipulator was mounted to a Pelican quadrotor host vehicle. The moving platform of the parallel manipulator was outfitted with a Point Gray Firefly MV [20] camera fit with a $2.4\ mm$ focal length lens to provide input for the eye-in-hand image based visual servoing controller that is responsible for positioning the manipulator relative to the target. Two sets of experiments were conducted. The first set included an evaluation of just the ability for the visual servoing system to maintain a pose relative to a fixed target despite perturbations to the host quadrotor. These perturbations were introduced by imperfections in the way a human pilot positioned the host UAV, and also in the form of wind generated by an industrial fan positioned to the side of the UAV. The second set of experiments made use of the partitioning algorithm to allow differences between the manipulator's current and desired position to be reduced by automatically controlling the host UAV's velocity.

A. Evaluation of Visual Servoing to Compensate for Host Perturbations

For this evaluation, the host UAV was commanded to maintain a pose relative to a fixed target that is used for visual servoing. Two experiments were run, one with still air conditions, and one with a cross wind of $6\ m/s$. The host UAV was manually flown by a safety pilot aided by

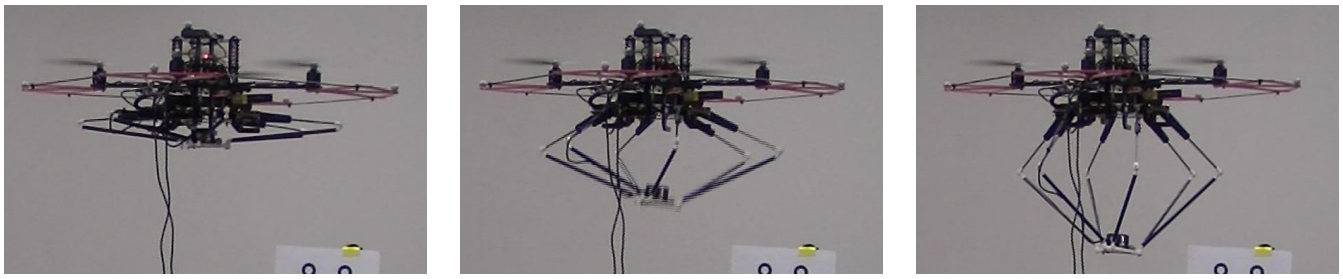

(a) Stowed (b) Transition (c) Deployed

Fig. 4. The parallel manipulator is designed so that it can stow for takeoff, translating flight and landing, and deploy for use

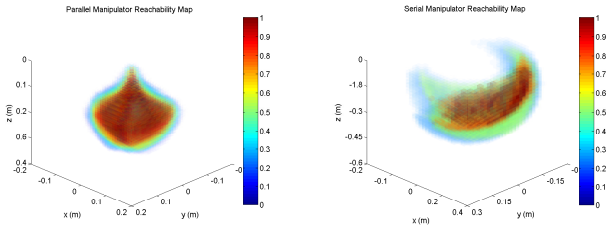

(a) Parallel (b) Serial

Fig. 5. Reachable poses of the parallel and serial manipulators. The colors represent the proportion of successes to attempts for reaching a goal orientation in each cell.

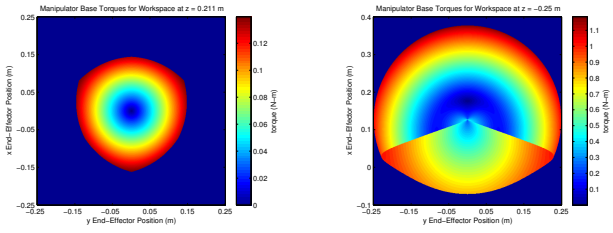

(a) Parallel manipulator (b) Serial manipulator

Fig. 6. Static manipulator torques for end-effector poses in the plane specified by the z component of ${}^{b\dagger}T_E$ for each manipulator

TABLE VI

RMS ERRORS OF THE CAMERA WHILE TRACKING A FIXED TARGET WITH AND WITHOUT CROSS-WIND IN THE $-y$ DIRECTION

Direction	RMSE (m) Camera, Still Air	RMSE (m) Camera, Wind
x	0.010	0.022
y	0.019	0.029
z	0.005	0.013

an IBVS controller that drove the manipulator and helped manuver the host UAV.

The RMS errors of the camera as shown in Table VI provide a model for how precisely an end-effector can be placed relative to a target using this system with and without wind perturbations. The position of the safety pilot controlled host UAV along with the position of the camera and target can be seen in Figures 7 and 8. From these plots, and the

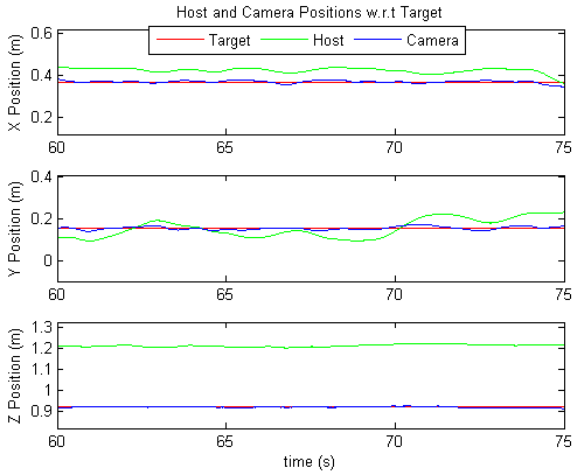

Fig. 7. Position of the quadrotor (host) and camera relative to a fixed target, tested without cross wind

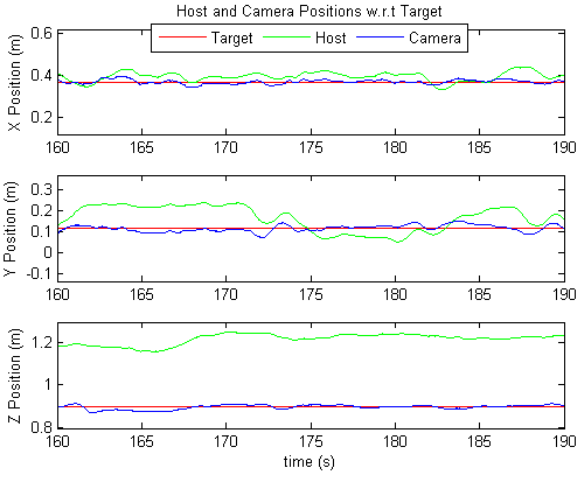

Fig. 8. Position of the quadrotor (host) and camera relative to a fixed target, tested with cross wind blowing toward the $-y$ direction

data shown in Table VI, it can be seen that the camera can be positioned more precisely than the positioning precision of the host UAV as shown in Table I.

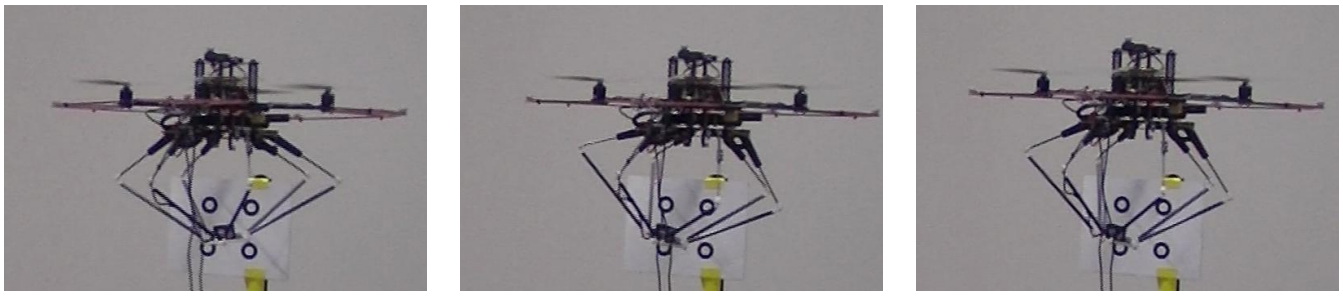

Fig. 9. System tracking stationary target with cross wind

VIII. Conclusions

Several conclusions are drawn from the material presented in this paper. Analysis shown in Section I shows that in the absence of pristine motion capture reference data, UAV positioning precision is so poor that grippers mounted directly to UAVs must either be unacceptably large or subject very low probabilities of successfully grasping simple objects. The use of six DOF parallel manipulators described in Section II, coupled with partitioned control algorithms allow for the system to perform end-effector positioning tasks despite perturbations to the host UAV position with a high degree of precision as demonstrated in Section VII. The characteristics of a manipulator to support these high precision end-effector placement tasks are described in Section VI and include the necessity for the manipulator to possess faster dynamics than those of the host UAV in addition to low overall weight and minimal moving mass. The integration of a manipulator with an aerial platform is further facilitated by considering manipulator configurations that allow for easy take off, landing and forward flight as well as resistance to crash damage.

A. Future Work

Aerial manipulation is an exciting and rapidly progressing field. The application of manipulating UAVs to truly useful tasks such as handling materials associated with industrial, civil, military or disaster response operations will soon be realized. While progress is constantly being made, more work must be performed before this vision may be realized. The parallel manipulator described in this work will serve as an excellent platform for further research, but it will benefit from design improvements such as increased rigidity and strength to make it more suitable for carrying grippers and performing interaction tasks such as peg-in-hole insertion, drilling and even hatch opening. Additionally, the visual servoing controller used for end-effector placement can be improved through the use of a larger set visual features and the fusion of higher rate inertial measurements to further improve positioning precision without contrived targets. Additional sensing modalities including radiation and acoustic may also be employed to provide precision measurements of non-visual environments. Overall, the contributions made by this and other recent works will lead to the use of aerial manipulation systems in ways that have not yet been imagined.

References

[1] Q. Lindsey, D. Mellinger, and V. Kumar, "Construction of cubic structures with quadrotor teams," *Proc. Robotics: Science & Systems VII*, 2011.

[2] N. Kuntz and P. Y. Oh, "Towards autonomous cargo deployment and retrieval by an unmanned aerial vehicle using visual servoing," in *Proceedings of 2008 ASME Dynamic Systems and Controls Conference*, 2008.

[3] M. Bernard and K. Kondak, "Generic slung load transportation system using small size helicopters," in *Robotics and Automation, 2009. ICRA'09. IEEE International Conference on*. IEEE, 2009, pp. 3258–3264.

[4] D. Mellinger, Q. Lindsey, M. Shomin, and V. Kumar, "Design, modeling, estimation and control for aerial grasping and manipulation," in *Intelligent Robots and Systems (IROS), 2011 IEEE/RSJ International Conference on*. IEEE, 2011, pp. 2668–2673.

[5] D. Mellinger, M. Shomin, N. Michael, and V. Kumar, "Cooperative grasping and transport using multiple quadrotors," in *Distributed autonomous robotic systems*. Springer, 2013, pp. 545–558.

[6] P. E. Pounds, D. R. Bersak, and A. M. Dollar, "Grasping from the air: Hovering capture and load stability," in *Robotics and Automation (ICRA), 2011 IEEE International Conference on*. IEEE, 2011, pp. 2491–2498.

[7] A. Torre, D. Mengoli, R. Naldi, F. Forte, A. Macchelli, and L. Marconi, "A prototype of aerial manipulator," in *Intelligent Robots and Systems (IROS), 2012 IEEE/RSJ International Conference on*. IEEE, 2012, pp. 2653–2654.

[8] S. Kim, S. Choi, and H. J. Kim, "Aerial manipulation using a quadrotor with a two dof robotic arm," in *IEEE/RSJ International Conference on Intelligent Robots and Systems*, Tokyo, Japan, 2013.

[9] J. Scholten, M. Fumagalli, S. Stramigioli, and R. Carloni, "Interaction control of an uav endowed with a manipulator," in *Robotics and Automation (ICRA), 2013 IEEE International Conference on*, May 2013, pp. 4910–4915.

[10] M. Fumagalli, R. Naldi, A. Macchelli, R. Carloni, S. Stramigioli, and L. Marconi, "Modeling and control of a flying robot for contact inspection," in *Intelligent Robots and Systems (IROS), 2012 IEEE/RSJ International Conference on*, Oct 2012, pp. 3532–3537.

[11] V. Lippiello and F. Ruggiero, "Cartesian impedance control of a uav with a robotic arm," in *10th IFAC Symposium on Robot Control International Federation of Automatic Control*, September 5-7, 2012.

[12] M. Orsag, C. Korpela, S. Bogdan, and P. Oh, "Valve turning using a dual-arm aerial manipulator," in *Unmanned Aircraft Systems (ICUAS), 2014 International Conference on*. IEEE, 2014, pp. 836–841.

[13] C. Korpela, P. Brahmbhatt, M. Orsag, and P. Oh, "Towards the realization of mobile manipulating unmanned aerial vehicles (mm-uav): Peg-in-hole insertion tasks," in *Technologies for Practical Robot Applications (TePRA), 2013 IEEE International Conference on*. IEEE, 2013, pp. 1–6.

[14] F. Huber, K. Kondak, K. Krieger, D. Sommer, M. Schwarzbach, M. Laiacker, I. Kossyk, S. Parusel, S. Haddadin, and A. Albu-Schaffer, "First analysis and experiments in aerial manipulation using fully actuated redundant robot arm," in *Intelligent Robots and Systems (IROS), 2013 IEEE/RSJ International Conference on*. IEEE, 2013, pp. 3452–3457.

[15] M. Achtelik, S. Weiss, and R. Siegwart, "Onboard imu and monocular vision based control for mavs in unknown in-and outdoor environments," in *Robotics and automation (ICRA), 2011 IEEE international conference on*. IEEE, 2011, pp. 3056–3063.

[16] P. Y. Oh and K. Allen, "Visual servoing by partitioning degrees of freedom," *Robotics and Automation, IEEE Transactions on*, vol. 17, no. 1, pp. 1–17, 2001.

[17] D. Stewart, "A platform with six degrees of freedom," *Proceedings of the institution of mechanical engineers*, vol. 180, no. 1, pp. 371–386, 1965.

[18] A. Keemink, M. Fumagalli, S. Stramigioli, and R. Carloni, "Mechanical design of a manipulation system for unmanned aerial vehicles," in *Robotics and Automation (ICRA), 2012 IEEE International Conference on*. IEEE, 2012, pp. 3147–3152.

[19] "Hitec hs-85bb+ micro servo," http://hitecrcd.com/products/servos/micro-and-mini-servos/analog-micro-and-mini-servos/hs-85bb-premium-micro-servo/product, accessed: 2014-09-17.

[20] "Point Gray firefly mv camera," http://ww2.ptgrey.com/USB2/fireflymv, accessed: 2014-09-4.